Effect of plasma-induced oxidative stress on the glycolysis pathway of Escherichia coli

Effect of plasma-induced oxidative stress on the glycolysis pathway of *Escherichia coli*

S. Ranjbar[1, 2]*, M. Shahmansouri[1], P. Attri[2, 3], A. Bogaerts[2]

[1] *Department of Physics, Faculty of Science, Arak University, Arak, 38156-8-8349, Iran*
[2] *Research group PLASMANT, University of Antwerp, Department of Chemistry, Universiteitsplein 1, Wilrijk-Antwerp, B-2610, Belgium*
[3] *Center of Plasma Nano-interface Engineering, Kyushu University, Fukuoka 819-0395, Japan*

Abstract

Antibiotic resistance is one of the world's most urgent public health problems. Due to its antibacterial properties, cold atmospheric plasma (CAP) may serve as an alternative method to antibiotics. It is claimed that oxidative stress caused by CAP is the main reason of bacteria inactivation. In this work, we computationally investigated the effect of plasma-induced oxidation on various glycolysis metabolites, by monitoring the production of the biomass. We observed that in addition to the significant reduction in biomass production, the rate of some reactions has increased. These reactions produce anti-oxidant products, showing the bacterial defense mechanism to escape the oxidative damage. Nevertheless, the simulations show that the plasma-induced oxidation effect is much stronger than the defense mechanism, causing killing of the bacteria.

Keywords: cold atmospheric plasma, oxidative stress, glycolysis pathway, bacteria killing, COBRA Toolbox

……

Corresponding authors: *E-mail: samiraranjbar1990@gmail.com;

1. Introduction

According to the European Center for Disease Prevention and Control Report in 2018, every year 33000 people die in Europe due to infections with antibiotic-resistant bacteria [1]. This illustrates the need for alternative methods to kill bacteria, such as photo-thermal (graphene-based, silver-based, gold-based, or $Fe_2O_3^+$gold based) [2-5] and bioelectric approaches [6, 7], as well as cold atmospheric plasma (CAP) [8].

CAP is an ionized gas produced at room temperature, in which heavy particles (such as gas molecules, atoms, radicals, ions) and electrons are in thermal non-equilibrium, i.e., the electrons have a much higher temperature than the heavy particles. It is usually produced in a rare gas flowing into ambient air, or directly in air, producing reactive oxygen species (ROS), such as superoxide anion (O_2^-), hydroxyl radicals (OH), singlet oxygen ($^1O_2$), hydrogen peroxide (H_2O_2), and ozone (O_3), as well as reactive nitrogen species (RNS), such as nitric oxide (NO), nitrogen dioxide (NO_2), nitrous oxide (N_2O), and nitrogen trioxide (NO_3) [9].

CAP has shown promising activity against bacteria, which is attributed to these reactive species [10-19]. Machala *et al.* reported that in particular ROS play a dominant role in decontamination of water [10]. Molecular dynamics simulations showed that O, OH, HO_2 radicals and H_2O_2 molecules can react with the bacterial cell wall, giving rise to the destruction of these bio-molecules [11], which might lead to bacteria killing. Attri *et al.* [15] investigated the effect of ROS/RNS on thermophilic bacterial proteins. Thermophilic bacteria are resistant to heat and chemicals, and it is difficult to destroy them with conventional methods Authors reported that CAP treatment modifies the protein structure and oxidizes the amino acids.

Among all bacteria, Escherichia coli (*E. coli*) is considered as a model system in fundamental biological and microbiological studies, and is used in various biotechnological applications [20]. The ability of E. coli to grow in specific chemical environments, as well as detailed genetic information about this bacterium, has made it an essential system in the study of the metabolic network [21, 22]. Joshi *et al.* [12] reported that plasma-treated *E. coli* bacteria undergo severe morphological changes due to oxidative stress. Plasma-induced lipid peroxidation yields byproducts that often react with DNA and proteins, leading to oxidative modifications, DNA damage and cell death. Vojusevic *et al.* [13] treated *E. coli* by oxygen plasma, and reported that the bacteria were fully destroyed after 2 minutes of exposure. SEM images of the bacteria showed cell wall damage after 1 minute of treatment. Hong *et al.* [14]

have shown drastic changes in the *E. coli* structure after oxygen plasma treatment. Yost *et al*. [16] reported that phosphate-buffered saline (PBS) solutions have strong antimicrobial properties. They found that plasma treatment of *E. coli* leads to and severe oxidative DNA damage. Dezest *et al*. [23] studied the modification of *E. coli* due to *He*, He/N_2 and He/O_2 plasma treatment. For He/O_2 even 30 seconds exposure was enough to completely inactivate the bacteria. Shaw *et al*. [18] demonstrated that a high concentration of both NO_2^- and H_2O_2 created by plasma is important for *E. coli* bacterial inactivation, through the creation of other RONS, such as O_2NOOH and $O_2^{\bullet-}$. Zhang *et al*. [19] studied the effect of plasma exposure on membrane proteins and intracellular proteins of *E. coli*.

The chemical composition of the bacterial environment is also an important factor in plasma treatment of bacteria. Privat-Maldonado *et al*. [24] indicated that since environmental substances are active participants in the treatment process, their reactions must be deliberated for precise elucidation of the results. They reported that the oxidation-reduction reactions of CAP-generated RONS with external organic biomolecules lead to generation of secondary RONS. Additionally, many studies have shown that plasma treatment oxidizes organic components present in cell culture media, which enhances the anticancer activity [9, 25-28].

The above studies are very interesting and reveal the oxidation of organic molecules present in the environment by plasma treatment might be responsible for the killing effect. However, knowledge on the bactericidal effect of different oxidized organic molecules is very limited. Therefore, in this study we try to understand the effect of oxidized glucose, by computational modeling.

E. coli is a smart bacterium, which might find alternative paths to escape from oxidative stress. Thus, we want to study the behavior of *E. coli* when it is expose to plasma. Glycolysis is one of the most important and vital pathways in cells since it provides the required energy [29]. Therefore, in this paper we investigate the possible effect of plasma-induced oxidation on biomolecules present in the glycolysis pathway and we monitor the change in biomass during oxidative stress. The bacterial biomass is obtained from experiments, and the flux of the reaction is obtained in such a way that the bacterium is in its exponential growth phase (see details in section 2.2).

We perform this study by computer simulations, using the constraint-based reconstruction and analysis (COBRA) Toolbox [30]. COBRA is a method widely used for

genome-scale modeling of metabolic networks in both prokaryotes and eukaryotes. Wang [22] comprehensively described the rules governing the COBRA Toolbox and also in Ref. [30, 31] the rules are explained step by step. COBRA is a constraint-base reconstruction algorithm, and using simple rules it tries to explain the behavior of the cell. COBRA enables us to identify what happens in the whole cell when something changes in a specific part. The number of biomedical applications of COBRA has been growing continuously. Ref. [32] provides a good review on using COBRA to investigate the cancer metabolism. The studies reported in that review paper demonstrate that constraint-based modeling can contribute significantly to systems biomedicine and personalized health care.

COBRA has been used to obtain *E. coli* mutants capable to produce succinate from renewable resources [33], to characterize the potential for *E. coli* to produce commodity chemicals [34], to apply developments in metabolic engineering strategies for advanced biofuel production using different hosts [35], to identify knockout reactions for maximizing the production of desired metabolites and the growth rate [36], to implement some strategies towards optimal violacein biosynthesis [37], to characterize the physiological responses to 22 gene knockouts in *E. coli* central carbon metabolism [38], to find effective compounds on metabolism by screening numerous available compounds [39], and for a lot of other applications [40-43].

We already know that disturbance of the glycolysis pathway in human beings triggers a form of cell death, called pyroptosis [44, 45]. Some articles revealed that similar changes in the bacterial glycolysis pathway can cause growth inhibition or cell death [46, 47]. To the best of our knowledge COBRA Toolbox has not been applied to investigate the effects of plasma-induced oxidative stress on the biomolecules present in the glycolysis pathway of *E. coli*, or any other bacteria.

2. Model description

2.1. E. coli core model in the COBRA Toolbox

We use the so-called *E. coli* strain K-12 sub-strain MG1655 core model [48]. This model contains 72 metabolites, 95 reactions and 137 genes. The following reactions take place in subsystems of this model: glycolysis/ gluconeogenesis, pentose phosphate pathway, oxidative phosphorylation, citric acid cycle, pyruvate metabolism, anaplerotic reactions, inorganic ion transport and metabolism, exchange reactions, etc. [29]. Perhaps the most crucial need of a cell is the generation and management of energy and reducing power. In our model, there are two main

mechanisms for ATP production (atp[c]) energy: 1) substrate-level phosphorylation, and 2) oxidative phosphorylation using the electron transport chain. When a specific pathway in the cell is a net producer of energy, we face substrate-level phosphorylation. In substrate level phosphorylation, atp[c] is produced from a reaction between ADP (adp[c]) and phosphorylated intermediate within the pathway. In our model these reactions take place in the glycolysis pathway. Hence, we apply plasma-induced oxidation to the glycolysis pathway metabolites, and we monitor its effect on the reaction rates in other pathways and also on the biomass production. A pathway indeed does not function in isolation, but in an entire network of interactions in the organism [22].

According to the *E. coli* core model, there are 12 reactions in the glycolysis pathway [29]. Considering also the exchange of glucose and the transport of glucose, there are 14 overall glycolysis-related reactions. Information on the metabolites is given in Table 1 and information on the reactions is shown in Table 2. The glycolysis pathway map, illustrating how these reactions are connected to each other, is presented in Figure 1. The other details of Table 2 are explained in the analysis section below.

Table 1: Glycolysis-related metabolites in *E. coli*

Abbr.	Metabolite	Formula
glc-D	D-Glucose	$C_6H_{12}O_6$
g6p	D-Glucose 6-phosphate	$C_6H_{11}O_9P$
f6p	D-Fructose 6-phosphate	$C_6H_{11}O_9P$
fdp	D-Fructose 1, 6-bisphosphate	$C_6H_{10}O_{12}P_2$
dhap	Dihydroxyacetone phosphate	$C_3H_5O_6P$
g3p	Glyceraldehyde 3-phosphate	$C_3H_5O_6P$
13dpg	3-Phospho-D-glyceroylphosphate	$C_3H_4O_{10}P_2$
3pg	3-Phospho-D-glycerate	$C_3H_4O_7P$
2pg	D-Glycerate-2-phosphate	$C_3H_4O_7P$
pep	Phosphoenolpyruvate	$C_3H_2O_6P$
pyr	Pyruvate	$C_3H_3O_3$
h	hydronium	H
h2o	water	H_2O
amp	Adenosine monophosphate	$C_{10}H_{12}N_5O_7P$
adp	Adenosine diphosphate	$C_{10}H_{12}N_5O_{10}P_2$
atp	Adenosine triphosphate	$C_{10}H_{12}N_4O_{13}P_3$
pi	Phosphate	HO_4P

nad	Nicotinamide adenine dinucleotide(NAD^+)	$C_{21}H_{26}N_7O_{14}P_2$
nadh	Nicotinamide adenine dinucleotide-reduced	$C_{21}H_{27}N_7O_{14}P_2$
accoa	Acetyl-CoA	$C_{23}H_{34}N_7O_{17}P_3S$
co2	CO_2	CO_2
coa	Coenzyme-A	$C_{21}H_{32}N_7O_{16}P_3S$

Table 2: Glycolysis-related reactions in *E. coli*

	ID[1]	Description	Reaction	Lower bound[2] (mmol /gDW. hr)	Upper bound[3] (mmol /gDW. hr)	Subsystem (compartment)
1	#28	EX-glc(e): D-Glucose exchange	$glc-D[e] \rightleftharpoons$ [4]	-1000	1000	Exchange
2	#50	GLCpts: D-glucose transport via pep: Pyr PTS	$glc-D[e] + pep[c] \rightarrow g6p[c] + pyr[c]$	0	1000	Transport, Extracellular
3	#74	PGI:glucose-6-phosphate isomerase	$g6p[c] \rightleftharpoons f6p[c]$	-1000	1000	Glycolysis/ Gluconeogenesis
4	#72	PFK: phosphofructokinase	$atp[c] + f6p[c] \rightarrow adp[c] + fdp[c] + h[c]$	0	1000	Glycolysis/ Gluconeogenesis
5	#41	FBP: fructose-bisphosphatase	$fdp[c] + h2o[c] \rightarrow f6p[c] + pi[c]$	0	1000	Glycolysis/ Gluconeogenesis
6	#40	FBA: fructose-bisphosphate aldolase	$fdp[c] \rightleftharpoons dhap[c] + g3p[c]$	0	1000	Glycolysis/ Gluconeogenesis
7	#95	TPI: triose-phosphate isomerase	$dhap[c] \rightleftharpoons g3p[c]$	-1000	1000	Glycolysis/ Gluconeogenesis
8	#49	GAPD: glyceraldehyde-3-phosphate dehydrogenase	$g3p[c] + nad[c] + pi[c] \rightleftharpoons 13dpg[c] + h[c] + nadh[c]$	-1000	1000	Glycolysis/ Gluconeogenesis
9	#75	PGK: phosphoglycerate kinase	$3pg[c] + atp[c] \rightleftharpoons 13dpg[c] + adp[c]$	-1000	1000	Glycolysis/ Gluconeogenesis

[1] ID given to the reactions in the *E. coli* core model
[2] Minimum allowable flux in a reaction (lower bound of the reactions potential flux, lower bound of reaction rate)
[3] Maximum allowable flux in a reaction (upper bound of the reactions potential flux, upper bound of reaction rate)
[4] Exchange reactions only have one side (reactions that move metabolites across in silico compartments)

10	#77	PGM: phosphoglycerate mutase	$2pg[c] \rightleftharpoons 3pg[c]$	-1000	1000	Glycolysis/ Gluconeogenesis
11	#18	ENO: enolase	$2pg[c] \rightleftharpoons h2o[c] + pep[c]$	-1000	1000	Glycolysis/ Gluconeogenesis
12	#83	PYK: pyruvate kinase	$adp[c] + h[c] + pep[c] \rightarrow atp[c] + pyr[c]$	0	1000	Glycolysis/ Gluconeogenesis
13	#81	PPS: phosphoenolpyruvate synthase	$atp[c] + h2o[c] + pyr[c] \rightarrow amp[c] + 2\,h\,c] + pep[c] + pi[c]$	0	1000	Glycolysis/ Gluconeogenesis
14	#71	PDH: pyruvate dehydrogenase	$coa[c] + nad[c] + pyr[c] \rightarrow accoa[c] + co2[c] + nadh[c]$	0	1000	Glycolysis/ Gluconeogenesis

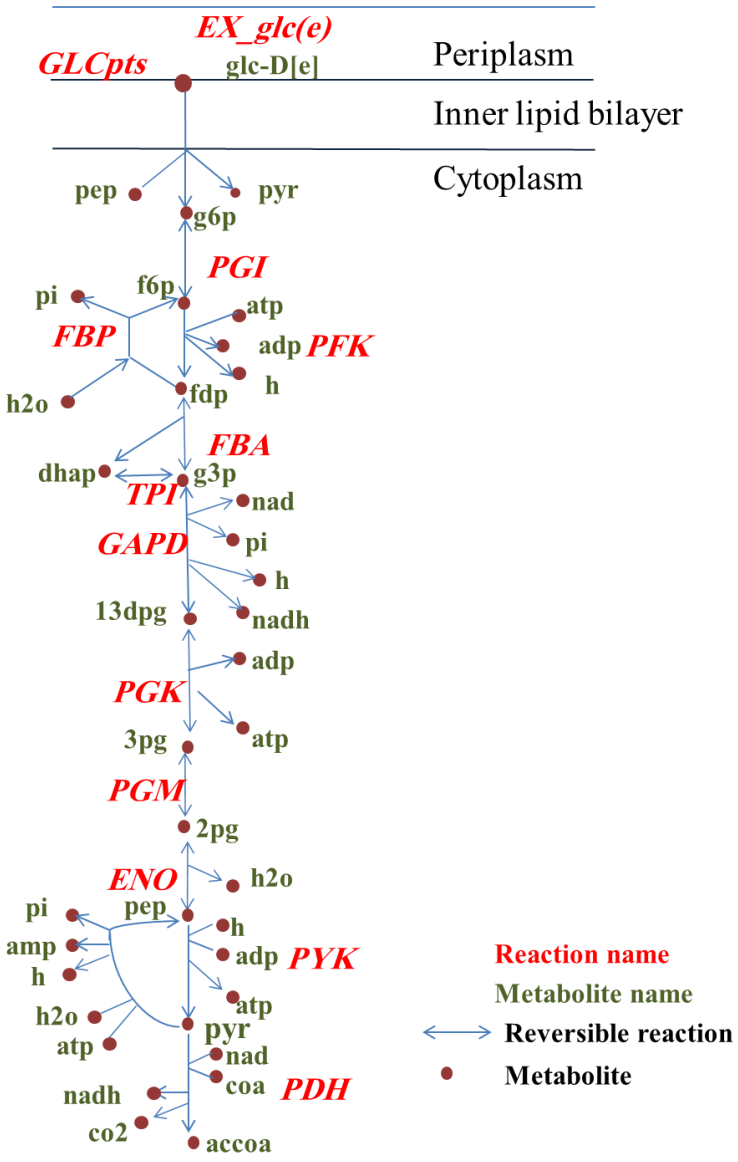

Figure 1: Glycolysis pathway map in the *E. coli* core model

2.2. Flux Balance Analysis (FBA) and Dynamic Flux Balance Analysis (dFBA)

The bacterial biomass is calculated as follows [29] (see abbreviations in Table 1): Biomass-Ecoli-core-w-GAM: 1.496 3pg[c] + 3.7478 accoa[c] + 59.81 atp[c] + 0.361 e4p[c] + 0.0709 f6p[c] + 0.129 g3p[c] + 0.205 g6p[c] + 0.2557 gln-L[c] + 4.9414 glu-L[c] + 59.81 h2o[c] + 3.547 nad[c] + 13.0279 nadph[c] + 1.7867 oaa[c] + 0.5191 pep[c] + 2.8328 pyr[c] + 0.8977

r5p[c] →59.81 adp[c] + 4.1182 akg[c] + 3.7478 coa[c] + 59.81 h[c] + 3.547 nadh[c] + 13.0279 nadp[c] + 59.81 pi[c].

Flux balance analysis (FBA) is a commonly used technique in metabolic systems. In this approach, for the quantitative estimation of the metabolic fluxes, a linear programming can be used to solve a system of linear equations for obtaining an objective function (e.g. biomass production: a reasonable weighted summation of the molecules that make new cells in the exponential growth phase) by the assumption of a steady-state under different constraints. If the change in biomass is the objective function, then the FBA analysis corresponds to the growth rate of the cell. The constraint can be applied in two ways: (i) a stoichiometric matrix which imposes mass balance constraint and (ii) the boundary condition which shows the allowable upper and lower bounds of the flux [29]. In FBA the constraints of the problem depict the space of all eligible possibilities from which an optimal solution can be selected. The output of FBA is a particular flux distribution, which maximizes or minimizes the objective function (e.g., biomass production) and stands between upper and lower bounds. Since FBA does not need kinetic parameters, the computation is very quick, even for large networks [29]. The steady-state approximation is generally valid because of fast equilibration of the metabolite concentrations (seconds) with respect to the time scale of genetic regulation (minutes) [49]. In our study, we apply some constraint to the boundary condition and calculate the objective function (biomass production - a linear function). We have used the FBA method because this method is most suitable when the problem involves a linear set of constraints.

In the COBRA Toolbox, it is possible to change the energy source of bacteria to 13 different organic substrates and calculate the maximum growth rate in aerobic and anaerobic conditions. The maximum growth rate in both aerobic and anaerobic conditions is reached for D-glucose substrate. Therefore, we consider D-glucose as substrate and we perform the simulations for aerobic conditions. All the simulations are carried out by MATLAB 2016b (COBRA Toolbox v.3– gurobi solver). As mentioned above, we consider the biomass production as the objective function. Hence, we study how the bacteria struggle to maximize their growth rate. In addition, we have also considered the glucose exchange reaction as the objective function, because we want to obtain information on maximum glucose uptake of *E. coli*.

Despite the many benefits of the FBA, this method also has some limitations. For instance, it cannot predict the change of the metabolic network as a function of time, in which we are

interested as well. Based on the method described by Varma and Palsson [50], Mahadevan *et al.* [51] developed the dynamic flux balance analysis (dFBA), which implements both dynamic and static optimization of an objective function.

One way to understand how the cell works is to visualize the cell's function through a metabolic map. Figure 2 illustrates the *E. coli* core map, with no limitation on boundary conditions (i.e., glucose and oxygen uptake is set to -1000 mmol/gDW.hr), to provide the maximum biomass production. As can be seen in Figure 2, glucose and oxygen enter the system (red color). The flux (reaction rate) through each reaction of this network is listed in Table 3. A complete insight into the *E. coli* core map is provided in Ref. [29]. A positive flux will remove the metabolite from the system, while a negative flux will add it into the system. The glucose exchange reaction (EX-glc(e); nr. 28 in Table 3) has a negative flux, so glucose enters the system and starts the glycolysis pathway. The color bar at the bottom of the map helps to qualitatively compare the value of the fluxes in the map. We will explain the map in detail in the Supporting information.

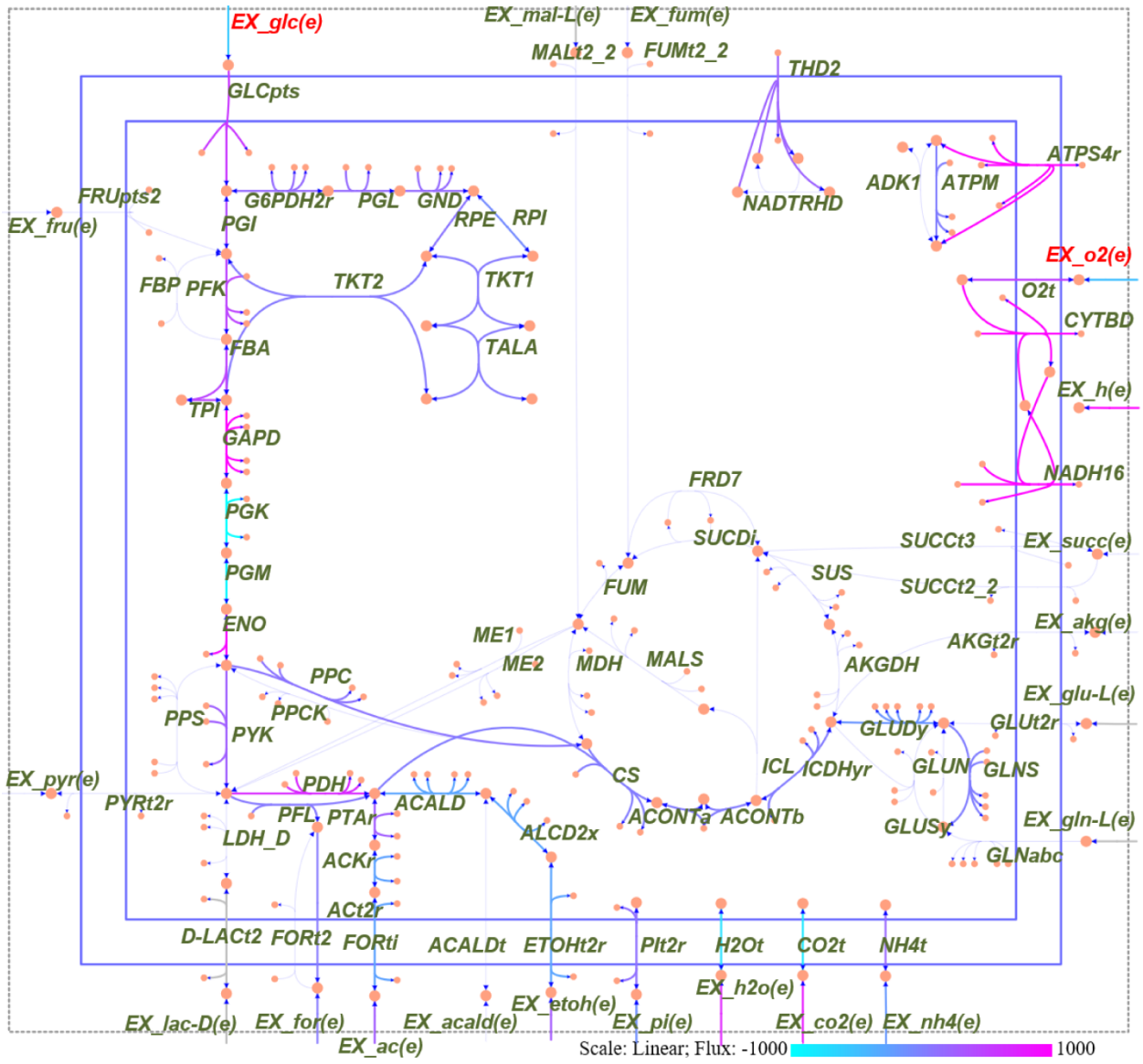

Figure 2: *E. coli* core map, when there is no limitation on boundary conditions, and the biomass production is set to be maximized (active reactions are shown in thick line and reactive reactions are shown in thin line). Details of this map are explained in the Supporting information.

Table 3: Flux in all of reactions in *E. coli* core model when there is no limitation for the reactions (glucose and oxygen uptake are both set to -1000 mmol/gDW.hr).

Reaction		Flux (mmol/g DW.hr)	Reaction		Flux (mmol/g DW.hr)	Reaction		Flux (mmol/g DW.hr)	Reaction		Flux (mmol/g DW.hr)
1	ACALD	-296.8	26	EX-fru(e)	0	51	GLNS	8.706	76	PGL	179.9
2	ACALDt	0	27	EX-fum(e)	0	52	GLNabc	0	77	PGM	-949.1
3	ACKr	-276.3	28	EX-glc(e)	-575.2	53	GLUDy	-176.9	78	PIt2r	125.2
4	ACONTa	36.73	29	EX-gln-L(e)	0	54	GLUN	0	79	PPC	97.57
5	ACONTb	36.73	30	EX-glu-L(e)	0	55	GLUSy	0	80	PPCK	0

6	ACt2r	-276.3	31	EX-h(e)	1000	56	GLUt2r	0	81	PPS	0
7	ADK1	0	32	EX-h2o(e)	767	57	GND	179.9	82	PTAr	276.3
8	AKGDH	0	33	EX-lac-D(e)	0	58	H2Ot	-767	83	PYK	258.6
9	AKGt2r	0	34	EX-mal-L(e)	0	59	ICDHyr	36.73	84	PYRt2r	0
10	ALCD2x	-296.8	35	EX-nh4(e)	-185.7	60	ICL	0	85	RPE	95.49
11	ATPM	8.39	36	EX-o2(e)	-500	61	LDH-D	0	86	RPI	-84.45
12	ATPS4r	1000	37	EX-pi(e)	-125.2	62	MALS	0	87	SUCCt2-2	0
13	Biomass-Ecoli-core-w-GAM	34.05	38	EX-pyr(e)	0	63	MALt2-2	0	88	SUCCt3	0
14	CO2t	-815.8	39	EX-succ(e)	0	64	MDH	0	89	SUCDi	0
15	CS	36.73	40	FBA	481.4	65	ME1	0	90	SUCOAS	0
16	CYTBD	1000	41	FBP	0	66	ME2	0	91	TALA	53.89
17	D-LACt2	0	42	FORt2	0	67	NADH16	1000	92	THD2	223.9
18	ENO	949.1	43	FORti	40.73	68	NADTRHD	0	93	TKT1	53.89
19	ETOHt2r	-296.8	44	FRD7	0	69	NH4t	185.7	94	TKT2	41.6
20	EX-ac(e)	276.3	45	FRUpts2	0	70	O2t	500	95	TPI	481.4
21	EX-acald(e)	0	46	FUM	0	71	PDH	696.6			
22	EX-akg(e)	0	47	FUMt2-2	0	72	PFK	481.4			
23	EX-co2(e)	815.8	48	G6PDH2r	179.9	73	PFL	40.73			
24	EX-etoh(e)	296.8	49	GAPD	1000	74	PGI	388.3			
25	EX-for(e)	40.73	50	GLCpts	575.2	75	PGK	-1000			

Since the COBRA Toolbox works in the exponential phase (as explained above), the biomass should increase with increasing glucose consumption, and thus with time (decreasing glucose concentration over time) (see Figure 3).

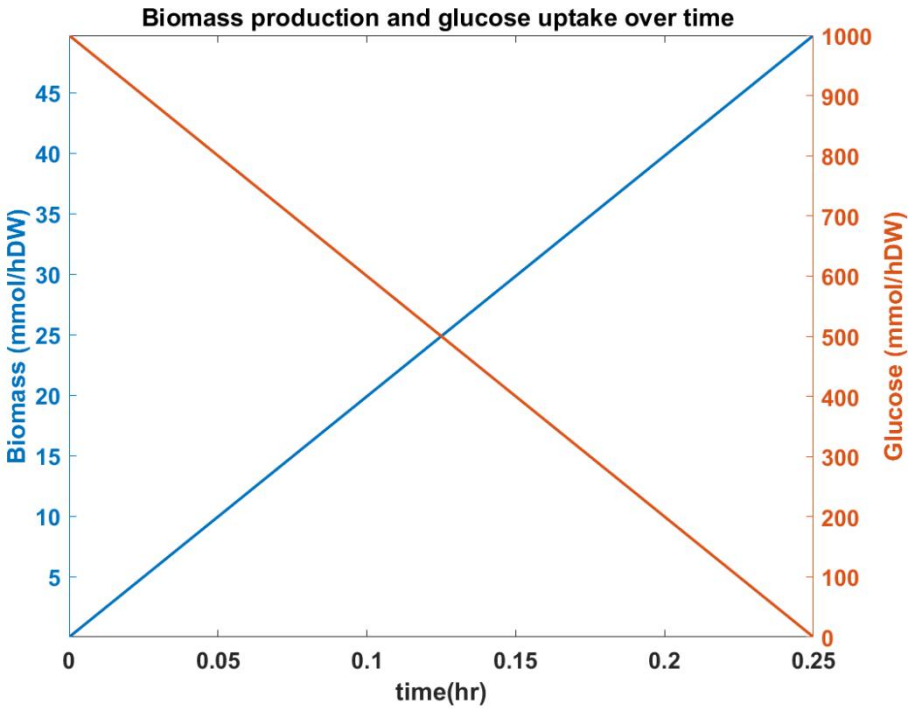

Figure 3: Biomass production (mmol/gDW.hr) and glucose concentration over time when the uptake of glucose and oxygen is unlimited (-1000 mmol/gDW.hr).

To obtain the optimized initial conditions for our simulation, we have set the glucose uptake as the objective function (i.e., the reaction that we aim to maximize) and we have used the optimize CbModel (i.e., a COBRA Toolbox function that optimizes the objective function). In addition, when the bacteria are exposed to the plasma species, we will have the highest amount of oxygen in the environment, so we have set the initial level of oxygen to -1000 mmol/gDW.hr for our simulation. The results of obtaining the optimized initial conditions for our simulation indicate that the maximum allowable value of glucose uptake is -10 mmol/gDW.hr and the biomass production is -0.8739 mmol/gDW.hr. We have thus set the glucose uptake to -10 mmol/gDW.hr and the oxygen uptake to -1000 mmol/gDW.hr, and we consider the biomass production (Biomass-E.coli-core-w-GAM; reaction 13 in Tables 2, 3 and 4) as the objective function (as initial condition), and we perform both FBA and dFBA. At these conditions, the biomass production and glucose consumption of *E. coli* are shown in Figure 4. We see that the glucose consumption is now initially slow, but its concentration drops faster after 2-3 hours. As a consequence, the biomass production is also slow in the beginning and rises exponentially. Because of the lower initial glucose concentration, the overall biomass production is much more

limited compared to Figure 3. The map of *E. coli* is presented in Figure 5. The important information in this map are the active pathways and the rate of each reaction in the map (as detailed in Table 4). We use the map in Figure 5 as a reference to compare the result of plasma-induced oxidation.

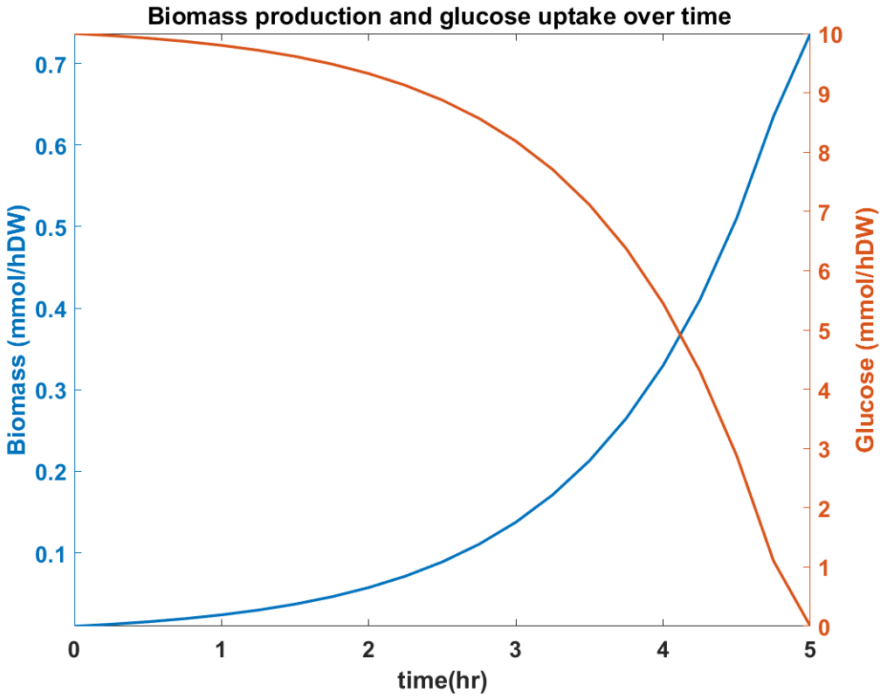

Figure 4: Biomass production and glucose concentration over time, when the uptake of glucose is limited to -10 mmol/gDW.hr and the oxygen uptake is unlimited (-1000 mmol/gDW.hr).

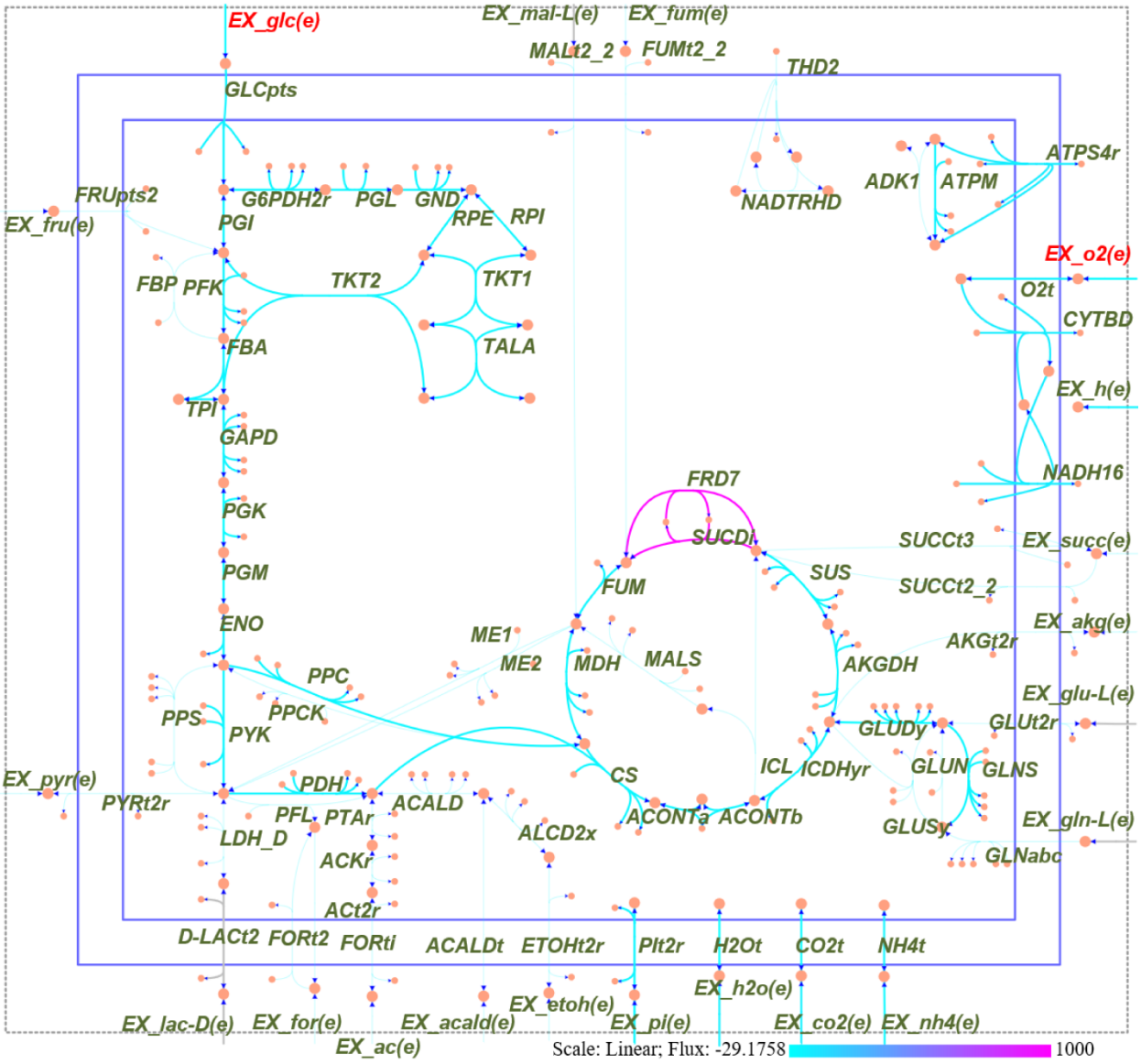

Figure 5: *E. coli* core map when the uptake of glucose is limited to -10 mmol/gDW.hr and the oxygen uptake is unlimited (-1000 mmol/gDW.hr). See detailed explanation in the Supporting information.

Table 4: Flux in all the reactions in the *E. coli* core model when the uptake of glucose is limited to -10 mmol/gDW.hr and the oxygen uptake is unlimited (-1000 mmol/gDW.hr).

Reaction		Flux (mmol/gDW.hr)	Reaction		Flux (mmol/gDW.hr)	Reaction		Flux (mmol/gDW.hr)	Reaction		Flux (mmol/gDW.hr)
1	ACALD	0	26	EX-fru(e)	0	51	GLNS	0.2235	76	PGL	4.96
2	ACALDt	0	27	EX-fum(e)	0	52	GLNabc	0	77	PGM	-14.72

3	ACKr	0	28	EX-glc(e)	-10	53	GLUDy	-4.542	78	PIt2r	3.215
4	ACONTa	6.007	29	EX-gln-L(e)	0	54	GLUN	0	79	PPC	2.504
5	ACONTb	6.007	30	EX-glu-L(e)	0	55	GLUSy	0	80	PPCK	0
6	ACt2r	0	31	EX-h(e)	17.53	56	GLUt2r	0	81	PPS	0
7	ADK1	0	32	EX-h2o(e)	29.18	57	GND	4.96	82	PTAr	0
8	AKGDH	5.064	33	EX-lac-D(e)	0	58	H2Ot	-29.18	83	PYK	1.758
9	AKGt2r	0	34	EX-mal-L(e)	0	59	ICDHyr	6.007	84	PYRt2r	0
10	ALCD2x	0	35	EX-nh4(e)	-4.765	60	ICL	0	85	RPE	2.678
11	ATPM	8.39	36	EX-o2(e)	-21.8	61	LDH-D	0	86	RPI	-2.282
12	ATPS4r	45.51	37	EX-pi(e)	-3.215	62	MALS	0	87	SUCCt2-2	0
13	Biomass-Ecoli-core-w-GAM	0.8739	38	EX-pyr(e)	0	63	MALt2-2	0	88	SUCCt3	0
14	CO2t	-22.81	39	EX-succ(e)	0	64	MDH	5.064	89	SUCDi	1000
15	CS	6.007	40	FBA	7.477	65	ME1	0	90	SUCOAS	-5.064
16	CYTBD	43.6	41	FBP	0	66	ME2	0	91	TALA	1.497
17	D-LACt2	0	42	FORt2	0	67	NADH16	38.53	92	THD2	0
18	ENO	14.72	43	FORti	0	68	NADTRHD	0	93	TKT1	1.497
19	ETOHt2r	0	44	FRD7	994.9	69	NH4t	4.765	94	TKT2	1.181
20	EX-ac(e)	0	45	FRUpts2	0	70	O2t	21.8	95	TPI	7.477
21	EX-acald(e)	0	46	FUM	5.064	71	PDH	9.283			
22	EX-akg(e)	0	47	FUMt2-2	0	72	PFK	7.477			
23	EX-co2(e)	22.81	48	G6PDH2r	4.96	73	PFL	0			
24	EX-etoh(e)	0	49	GAPD	16.02	74	PGI	4.861			
25	EX-for(e)	0	50	GLCpts	10	75	PGK	-16.02			

It is worth to notice that in this reference condition (when the uptake of glucose is -10 mmol/gDW.hr and the oxygen uptake is -1000 mmol/gDW.hr), the minimum flux (reaction rate) in the map (color bar in Figure 5) is -29.18 mmol/gDW.hr (H2Ot (transport of H_2O via diffusion); reaction 58 in Table 4) and the maximum flux (reaction rate) is 1000 mmol/gDW.hr (SUCDi; succinate dehydrogenase (irreversible); reaction 89 in Table 4).

2.3. Plasma oxidation of biomolecules in the glycolysis pathway

To evaluate the effect of oxidative damage caused by plasma, we have studied the natural oxidation of the entire glycolysis pathway reactions (i.e., oxidation of each reactant), and we have identified the reactants that are affected by plasma. Subsequently, we have changed the boundary conditions of some reactions due to their oxidation statuse. The flux of a reaction and the concentrations of its reactants are directly connected, so if the concentration of a reactant

drops by a factor ten, the flux (reaction rate) also drops by that same factor ten. We performed simulations for oxidation degrees varying from 10% to 90% (i.e., 10%, 20%, 30%, 40%, 50%, 60%, 70%, 80%, and 90%).

Only the following three reactions have an oxidation product. The first reaction is glucose exchange:

$$C_6H_{12}O_6 \rightleftharpoons \qquad (1)$$

In the reference conditions (without plasma exposure), the upper bound and lower bound of the glucose flux is 1000 mmol/gDW.hr and -10 mmol/gDW.hr, respectively (Table 4).

We want to know the effect of plasma on the first glycolysis reaction. As mentioned in the introduction, the main effect of plasma is supposed to be oxidation of biomolecules. The oxidation of glucose can be written as [52]:

$$C_6H_{12}O_6 + \frac{1}{2}O_2 \rightarrow C_6H_{12}O_7 \qquad (2)$$

The oxygen initial concentration determines the rate of the reaction. In case of plasma-induced oxidation, the initial condition is determined by plasma and can be considered the maximum possible amount. Indeed, as explained in the introduction, oxidative damage is the dominant effect of plasma, and it is not important how it is caused (by which species). We can thus simply treat all plasma species causing oxidation as being oxygen in this model, so the amount of oxygen is the maximum value. The product of this reaction is D-gluconic acid. When glucose is oxidized, we have to change the boundary condition of the glucose uptake. We assume the lower bound (uptake of reactant) between 10% and 90 % of its value before oxidation.

The other reaction in the glycolysis pathway is glucose-6-phosphate isomerization (PGI: reaction 74 from Table 2 and Table 3):

$$g6p[c](C_6H_{11}O_9P) \rightleftharpoons f6p[c](C_6H_{11}O_9P) \qquad (3)$$

Oxidation of glucose-6-phosphate (g6p) happens in several ways [53]. One of the oxidation reactions is:

$$g6p\,(C_6H_{11}O_9P) + 12nadp(C_{21}H_{25}N_7O_{17}P_3) + \rightarrow 12nadph(C_{21}H_{26}N_7O_{17}P_3) + Pi(HO_4P) + 6CO_2 \qquad (4)$$

(nadp: Nicotinamide-adenine-dinucleotide-phosphate, C21H25N7O17P3
nadph: Nicotinamide-adenine-dinucleotide-phosphate-reduced, C21H26N7O17P3)
We change the boundary condition of this reaction as explained for the glucose exchange reaction. The last reaction is pyruvate dehydrogenase (PDH reaction 71 from Table 2 and Table 3):

$$coa[c](C_{21}H_{32}N_7O_{16}P_3S) + nad[c](C_{21}H_{26}N_7O_{14}P_2) + pyr[c](C_3H_3O_3) \rightarrow accoa[c](C_{23}H_{34}N_7O_{17}P_3S) + co2[c] + nadh[c](C_{21}H_{27}N_7O_{14}P_2) \quad (5)$$

(accoa[c], Acetyl-CoA, C23H34N7O17P3S, coa[c], Coenzyme-A, C21H32N7O16P3S)
Coenzyme-A is made of pantothenic acid, which is a vitamin B (B_5) [54]. D-panthenol (2, 4-Dihydroxy-N-(3-hydroxypropyl)-3, 3- dimethylbutanamide) is the more stable alcohol form of pantothenic acid (Vitamin B5). Therefore, pantothenic acid is known as provitamin B5. Nayak *et al.* [55] used an electrochemical method for oxidation of provitamin B5. So there is an oxidized form of coenzyme-A and we can apply the limiting boundary condition to the last reaction.

Fructose-bisphosphate aldolase (FBA: reaction 40 in Table 2 and 3) and triose-phosphate isomerase (TPI; reaction 95 of Table 2 and Table 3) are reversible reactions, and we have to consider the oxidation of both the reactants and the products. There is no evidence on oxidation of these reactants, but in [56] there is some information about glyceraldehyde 3-phosphate (g3p) oxidation (phosphorylation).

$$g3p(C_3H_5O_6P) + nad(C_{21}H_{26}N_7O_{14}P_2) + Pi(HO_4P) \rightleftharpoons 1,3\ diphosphoglycerate(C_3H_8O_{10}P_2) + nadh(C_{21}H_{27}N_7O_{14}P_2) + H \quad (6)$$

This is the only oxidation reaction found for g3p, but this reaction is one of the reactions in the glycolysis pathway (GAPD; reaction 49 in Table 2 and 3). Hence, plasma-induced oxidation probably has just little effect on that reaction and will slightly increase the rate of phosphorylation. So we do not change the boundary condition of this reaction.

All other reactions (i.e. phosphofructokinase (PFK; reaction 72 of Table 2 and 3), fructose-bisphosphatase (FBP: reaction 41 in Table 2 and 3), phosphoglycerate kinase (PGK; reaction 75 in Table 2 and 3), phosphoglycerate mutase (PGM; reaction 77 in Table 2 and 3), enolase (ENO; reaction 18 in Table 2 and 3), pyruvate kinase (PYK; reaction 83 in Table 2 and 3), phosphoenolpyruvate synthase (PPS; reaction 81 in Table 2 and 3)), do not have any

oxidation products. It means that either they are reduced instead of oxidized (e.g. 3-phosphoglycerate) or there is no information on oxidation of either the reactants or the products, so we do not change anything about their oxidation in our model.

Results and Discussion

The purpose of this work is to study the effect of plasma-induced oxidation, more specifically for the above three oxidation reactions, on the biomass production. In the first reaction, glucose is oxidized (reaction (2) in section 2.3). We varied the glucose oxidation between 10% and 90%. The simulation results as a function of percentage of glucose oxidation are presented in the Supporting information (Table S1). The results for 90% glucose oxidation are shown in Figures S1 and S2 in the Supporting information. The first thing to notice in Figure S2 (in the color bar at the bottom of the map) is that the reaction rate in the whole network is reduced from about -29.19 mmol/gDW.hr in the standard condition (Figure 5) to -4.29 mmol/gDW.hr. It shows that oxidation of glucose in the extracellular compartment not only affects the reactions in the glycolysis pathway but also in the other pathways. However, the active pathways are similar to the active pathway of Figure 5. The difference between these two maps are the fluxes in each reaction or the reaction rates. The reaction rates in Figure S2 obviously reduce upon glucose oxidation.

In addition, the biomass production rate drops linearly upon increasing percentage of glucose oxidation (see Figure 6). Note: the map and biomass production at different percentages of oxidation are very similar: the trend of biomass production is the same, but the amount is different. The differences are clear from Figure 6 and Table S1 in the Supporting information.

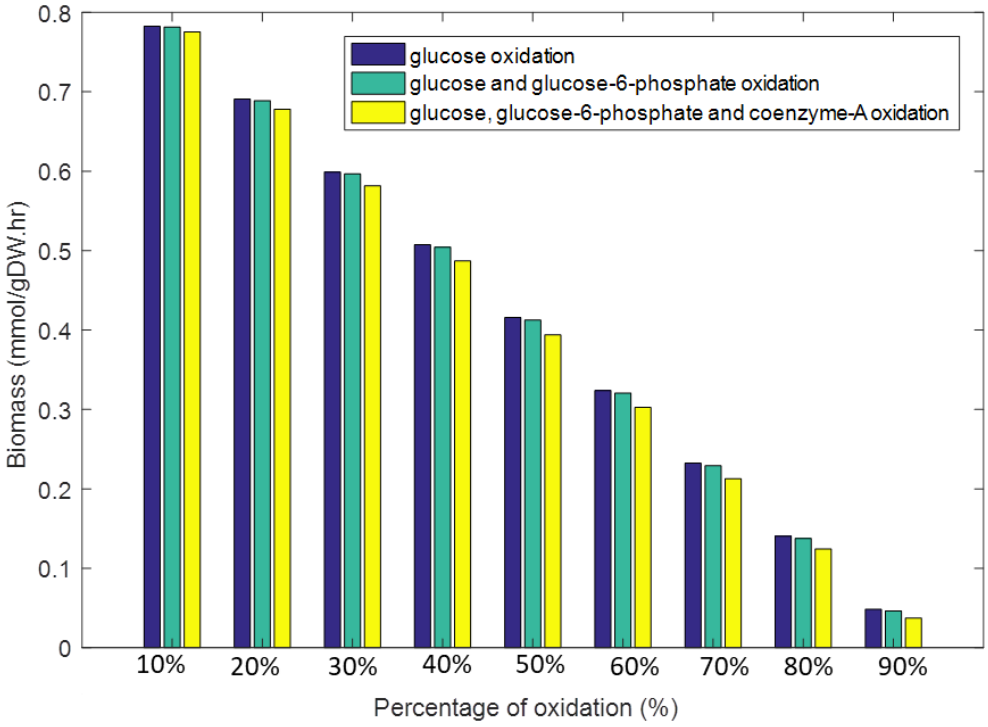

Figure 6: Biomass production as a function of percentage of oxidation of glucose, glucose-6-phosphate and coenzyme-A.

To understand the effect of oxidation by plasma, we consider all the reactions of which the rate changes due to a change in the rate of glucose exchange. There are 46 reactions (out of 95) of which the rates decrease due to plasma oxidation (see Figure 7), and two reactions of which the the rates increase (indicated with an asterix), while for the other 47 reactions the rates remain unchanged, and they are therefore not plotted in Figure 7. The reduction in the rate of these 46 reactions is directly attributed to the reduction in glucose concentration. However, the increase in the rate of the other two reactions may seem unexpected, so we focus on these two reactions.

The first reaction is fumarate reductase (FRD7; nr. 44 in Tables 3 and 4):

$$Fumarate(C_4H_2O_4) + Ubiquinol\ 8\ (C_{49}H_{76}O_4) \rightarrow Ubiquinone8(C_{49}H_{74}O_4) + Succinate(C_4H_4O_4) \qquad (6)$$

which converts furmarate to succinate and plays a role in anaerobic respiration. The rate of this reaction slightly increases from 994.9 mmol/gDW.hr in the reference condition to 998.7 mmol/gDW.hr after 90% of glucose oxidation. Some investigations confirm that the production of succinate increases under oxidative stress in the cell [57]. The conversion of fumarate into succinate is also markedly increased in cells under stress [58]. Indeed, succinate has antioxidant properties [59], and the increasing level of succinate is probably because of the defense mechanism against oxidative damage.

The other reaction is NAD transhydrogenase (NADTRHD; nr. 68 in Tables 3 and 4) of which the rate increases from zero in the reference condition to 0.435 mmol/gDW.hr after 90% of glucose oxidation:

$$Nicotinamide\ adenine\ dinucleotide, (C_{21}H_{26}N_7O_{14}P_2) + Nicotinamide\ adenine\ dinucleotide\ phosphate\ reduced\ (C_{21}H_{26}N_7O_{17}P_3) \rightarrow Nicotinamide\ adenine\ dinucleotide\ reduced (C_{21}H_{27}N_7O_{14}P_2)` + Nicotinamide\ adenine\ dinucleotide\ phosphate\ (C_{21}H_{27}N_7O_{14}P_2) \quad (7)$$

The rate of transhydrogenase production is also increased in this reaction, which may also be directly involved in the defense against oxidative stress [60].

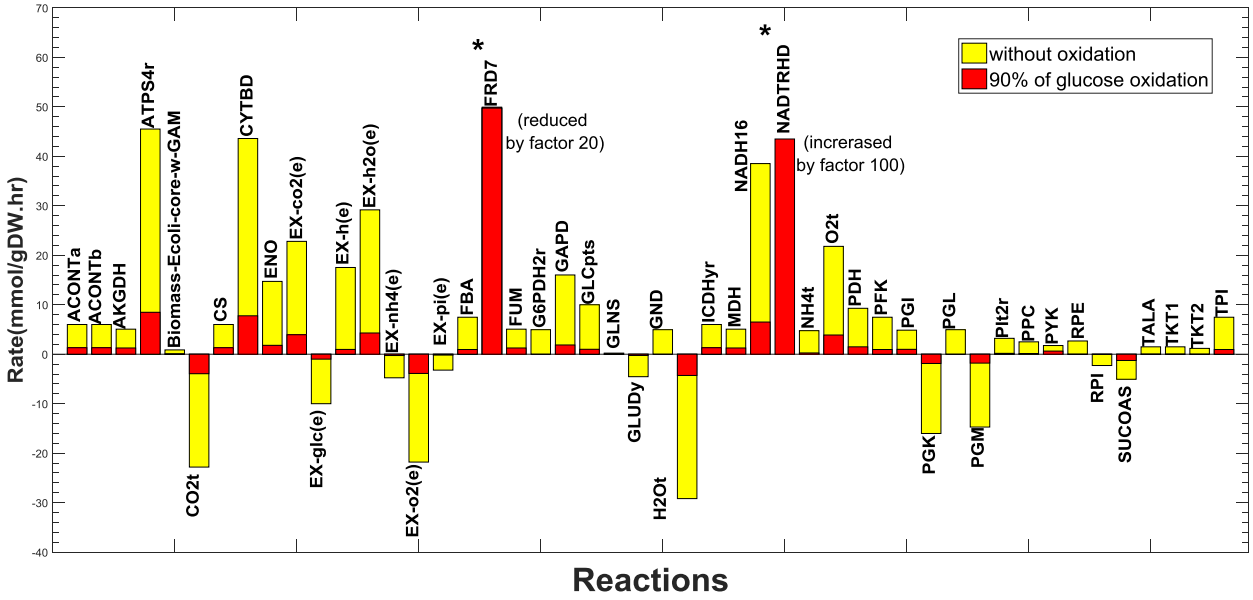

Figure 7: Rates of the reactions in the *E. coli* core model, without and with glucose oxidation. Only those reactions are plotted for which the rates drop or rise upon 90% glucose oxidation. For 46 reactions, the rates drop, while for two reactions (indicated with *, and different scale, to be visible in this scale) the rates increase. The reactions are plotted in the same order as they are listed in Tables 3 and 4 (but without the reactions for which the rates are unchanged).

Despite the significant reduction of biomass production (see Figure S1, compared to Figure 4), the first oxidation step (glucose oxidation) thus causes the activation of some defense mechanisms in *E. coli*. Increasing concentrations of antioxidant metabolites, i.e., succinate and transhydrogenase, without oxidation of their reactants directly, shows that the bacteria are trying to survive against oxidative stress, but nevertheless they cannot escape from the oxidative damage.

The second oxidation step is the oxidation of glucose-6-phosphate (reaction 4 in section 2.3), which is formed by the PGI (isomerization) reaction (reaction 3 in section 2.3). The rate of the PGI reaction before oxidation of glucose is 4.861 mmol/gDW.hr (Table 4; reaction nr.74), but after glucose oxidation the rate is reduced to the values presented in Table S1 in the

Supporting information (for different percentages of oxidation). The rates of the different reactions for different percentages of glucose-6-phosphate oxidation are presented in Table S2 of the Supporting information. The simulation results after 90% oxidation of both glucose and glucose-6-phosphate are shown in Figures S3 and S4 in the Supporting information The calculated biomass production as a function of percentage of glucose-6-phosphate oxidation (in addition to glucose oxidation) is also plotted in Figure 6.

The results show that oxidation of glucose-6-phosphate in the PGI reaction has little effect on the network and on the biomass production. This is probably because of the isomeric nature of the PGI reaction, i.e., oxidation of glucose-6-phosphate in this reaction only reduces the rate of conversion of glucose-6-phosphate to fructose-6-phosphate and does not affect the amount of fructose-6-phosphate, because this reactant is produced simultaneously through other reactions, e.g. FBP. As can be seen in Figure 6, the reduction of biomass production is indeed not as significant as for the glucose oxidation. It is also obvious that the rate of other reactions increases; see Table S2 (Supporting information).

At the last step we investigated the effect of oxidation of coenzyme-A (because of oxidation of provitamine B5 which is a part of coenzyme-A) in the PDH reaction (reaction 5 in section 2.3). The simulation results upon 90% oxidation of glucose, glucose-6-phosphate and coenzyme-A are shown in Figures S5 and S6 in the Supporting information. The other reaction rates are presented in Table S3. The calculated biomass production as a function of percentage of coenzyme-A oxidation is also plotted in Figure 6. The yellow bars are only slightly lower than the blue ones, so most effect is due to glucose oxidation, and coenzyme-A only has a little effect. However, its effect is slightly larger than oxidation of glucose-6-phosphate. Moreover, in this step the rate of the reactions is more dependent on the percentage of oxidation than in the previous ones (see Table S3 in the Supporting information). The results show that some reactions that used to have zero rate, are active now. Because most reactions have a non-zero rate, the rate of biomass production continues to decrease. Table 5 presents the reactions and their rates that are activated in this step and were not active in the previous steps, for 90% oxidation of coenzyme-A.

Table 5: Reactions that are activated in the last step (oxidation of coenzyme-A).

Abbr.	Description	Reaction	Lower bound	Upper bound	Subsystem	Reaction rates after oxidation of co-enzyme A (mmol/g.DW.hr)
ADK1	adenylate kinase	$amp[c] + atp[c] \rightleftharpoons 2\ adp[c]$	-1000	1000	Oxidative Phosphorylation	0.1747
EX-for(e)	Formate exchange	$for[e] \rightarrow$	0	1000	Exchange	0.5992
FORti	formate transport via diffusion	$for[c] \rightarrow for[e]$	0	1000	Transport, Extracellular	0.5992

PFL	pyruvate formate lyase	$coa[c] + pyr[c] \rightarrow accoa[c] + for[c]$	0	1000	Pyruvate Metabolism	0.5992
PPS	phosphoenolpyruvate synthase	$atp[c] + h2o[c] + pyr[c] \rightarrow amp[c] + 2\,h[c] + pep[c] + pi[c]$	0	1000	Glycolysis/ Gluconeogenesis	0.1747

Conclusion

In this work, we used a novel constraint-based approach, based on the assumption that cells struggle to maximize their growth rate, to monitor the behavior of *E. coli* under oxidative stress conditions. We evaluated the maximum growth rate by studying the maximum biomass production. In order to guarantee that the results for a predicted rate of reactions are valid, at least one of the reactions must be constrained. We apply constraints on our reactions according to the oxidation of reactants (and in reversible reactions, oxidation of both reactants and products). Subsequently, we analysed the rate of each reaction upon plasma-induced oxidation. Since the environment is important in oxidative damage, we have also considered the oxidation of glucose (as the environment). Through glucose oxidation, the rate of fumarate reductase and NAD transhydrogenase production is increased. The products of these reactions have antioxidant properties. At the same time, the biomass production is dramatically reduced. This confirms the experiments of Maldonado *et. al* [23], who observed that the environment is also important in oxidative damage. Oxidation of glucose-6-phosphate may cause a higher rate in some reactions, but the biomass production is still reduced. Upon oxidation of coenzyme-A, some of the reactions of which the rates were increased upon oxidation of glucose-6-phosphate are now reduced again. Oxidation thus seems to decrease or increase the rate of reactions, indicating that the bacteria activate their antioxidant defense mechanism again this oxidative stress, but the overall result is that the biomass production rate is always reduced, which means that the bacterial growth rate is reduced, or in otherwords, that the oxidation causes bacterial killing. The reduced growth rates in bacteria can results in disruption of glycolytic flux is a signal for inflammasome signaling and pyroptotic cell death, cited as reference [44]. In another report the Hazeline Roche-Hakansson *et. al* [61] showed that disruption in glycolysis, can induces death in Streptococcus pneumonia.

It is important to note that we only consider here the glycolysis pathway. Although oxidation in this pathway has a major impact on the biomass production, the latter has not yet

reached zero. Therefore, it would be interesting to see whether other pathways are also important. In addition, we could only apply constraints (i.e oxidation of reactant and product) if this information was available in literature. This also limits our study because other reactants or products in the glycolysis pathway might also be oxidized in reality. If information about such oxidation products becomes available in the future, we can further improve our modeling study.

To our knowledge, the COBRA Toolbox has not yet been used in plasma medicine research before. It does not require much calculation time compared to other methods, *e.g*. molecular dynamics (MD) simulations. We believe the COBRA Toolbox can be linked to MD methods by using the MD results as input to monitor the overall behavior of the cell. It would be interesting to investigate this in the future, not only for plasma sterilization purposes but also for other plasma medicine applications, like cancer treatment.

Acknowledgment

S. R. acknowledges funding from the Ministry of Science and Technology of Iran. The computational work was carried out using the Turing HPC infrastructure at the CalcUA core facility of the Universiteit Antwerpen (UA), a division of the Flemish Supercomputer Center VSC, funded by the Hercules Foundation, the Flemish Government (department EWI) and the UA. We also would like to thank Dr. Charlotta Bengtson for her suggestions in writing this paper.

References

[1] EuropeanCenterforDiseasePreventionandControl, Infographic: Antibiotic resistance – an increasing threat to human health Infographic, https://ecdc.europa.eu/en/publications-data/infographic-antibiotic-resistance-increasing-threat-human-health, (2018).
[2] M.-C. Wu, A.R. Deokar, J.-H. Liao, P.-Y. Shih, Y.-C. Ling, Graphene-Based Photothermal Agent for Rapid and Effective Killing of Bacteria, ACS Nano, 7 (2013) 1281-1290.
[3] W.-C. Huang, P.-J. Tsai, Y.-C. Chen, Functional gold nanoparticles as photothermal agents for selective-killing of pathogenic bacteria, Nanomedicine, 2 (2007) 777-787.
[4] K. Kalwar, D. Shan, Antimicrobial effect of silver nanoparticles (AgNPs) and their mechanism – a mini review, Micro & Nano Letters, Institution of Engineering and Technology, 2018, pp. 277-280.
[5] W.-C. Huang, P.-J. Tsai, Y.-C. Chen, Multifunctional Fe3O4@Au Nanoeggs as Photothermal Agents for Selective Killing of Nosocomial and Antibiotic-Resistant Bacteria, Small, 5 (2009) 51-56.
[6] J.W. Costerton, B. Ellis, K. Lam, F. Johnson, A.E. Khoury, Mechanism of electrical enhancement of efficacy of antibiotics in killing biofilm bacteria, Antimicrobial Agents and Chemotherapy, 38 (1994) 2803.
[7] H. Hülsheger, J. Potel, E.-G. Niemann, Killing of bacteria with electric pulses of high field strength, Radiation and Environmental Biophysics, 20 (1981) 53-65.

[8] M. Laroussi, D.A. Mendis, M. Rosenberg, Plasma interaction with microbes, New Journal of Physics, 5 (2003) 41-41.
[9] P. Attri, A. Bogaerts, Perspectives of Plasma-treated Solutions as Anticancer Drugs, Anti-Cancer Agents in Medicinal Chemistry- Anti-Cancer Agents), 19 (2019) 436-438.
[10] Z. Machala, L. Chládeková, M. Pelach, Plasma agents in bio-decontamination by dc discharges in atmospheric air, Journal of Physics D: Applied Physics, 43 (2010) 222001.
[11] A. Bogaerts, M. Yusupov, J. Van der Paal, C.C.W. Verlackt, E.C. Neyts, Reactive Molecular Dynamics Simulations for a Better Insight in Plasma Medicine, Plasma Processes and Polymers, 11 (2014) 1156-1168.
[12] S.G. Joshi, M. Cooper, A. Yost, M. Paff, U.K. Ercan, G. Fridman, G. Friedman, A. Fridman, A.D. Brooks, Nonthermal Dielectric-Barrier Discharge Plasma-Induced Inactivation Involves Oxidative DNA Damage and Membrane Lipid Peroxidation in <em>Escherichia coli</em&gt, Antimicrobial Agents and Chemotherapy, 55 (2011) 1053.
[13] D. Vujosevic, U. Cvelbar, U. Repnik, M. Modic, S. Lazovic, T. Zavasnik-Bergant, N. Puac, B. Mugosa, E. Gogolides, Z.L. Petrovic, M. Mozetic, Plasma effects on the bacteria Escherichia coli via two evaluation methods, Plasma Sci Technol, 19 (2017) 075504.
[14] Y.F. Hong, J.G. Kang, H.Y. Lee, H.S. Uhm, E. Moon, Y.H. Park, Sterilization effect of atmospheric plasma on Escherichia coli and Bacillus subtilis endospores, Lett Appl Microbiol, 48 (2009) 33-37.
[15] P. Attri, J. Han, S. Choi, E.H. Choi, A. Bogaerts, W. Lee, CAP modifies the structure of a model protein from thermophilic bacteria: mechanisms of CAP-mediated inactivation, Scientific Reports, 8 (2018) 10218.
[16] A.D. Yost, S.G. Joshi, Atmospheric Nonthermal Plasma-Treated PBS Inactivates Escherichia coli by Oxidative DNA Damage, PloS one, 10 (2015) e0139903-e0139903.
[17] M. Dezest, A.L. Bulteau, D. Quinton, L. Chavatte, M.L. Bechec, J.P. Cambus, S.p. Arbault, A. Nègre-Salvayre, F. Cle´ment, S. Cousty, Oxidative modification and electrochemical inactivation of Escherichia coli upon cold atmospheric pressure plasma exposure, PLOS ONE, DOI 10.1371/journal. pone.0173618(2017).
[18] P. Shaw, N. Kumar, H.S. Kwak, J.H. Park, H.S. Uhm, A. Bogaerts, E.H. Choi, P. Attri, Bacterial inactivation by plasma treated water enhanced by reactive nitrogen species, Scientific Reports, 8 (2018) 11268.
[19] H. Zhang, J. Ma, J. Shen, Y. Lan, L. Ding, S. Qian, W. Xia, C. Cheng, P.K. Chu, Roles of membrane protein damage and intracellular protein damage in death of bacteria induced by atmospheric-pressure air discharge plasmas, RSC Advances, 8 (2018) 21139-21149.
[20] S.Y. Lee, Systems Biology and Biotechnology of Escherichia coli, Springer Science & Business Media B.V.2009.
[21] J.E.E.c.a.a.E.O.I.e. Cronan, John Wiley & Sons, Ltd (Ed.).
doi:10.1002/9780470015902.a0002026.pub2, eLS.
[22] D. Wang, Systems Biology: Constraint-Based Reconstruction and Analysis by Bernhard O. Palsson, The University of Chicago Press2017.
[23] M. Dezest, A.L. Bulteau, D. Quinton, L. Chavatte, M. Le Bechec, J.P. Cambus, S. Arbault, A. Negre-Salvayre, F. Clement, S. Cousty, Oxidative modification and electrochemical inactivation of Escherichia coli upon cold atmospheric pressure plasma exposure, PLoS One, 12 (2017) e0173618.
[24] A. Privat-Maldonado, Y. Gorbanev, D. O'Connell, R. Vann, V. Chechik, M.W.v.d. Woude, Nontarget Biomolecules Alter Macromolecular Changes Induced by Bactericidal Low–Temperature Plasma, IEEE Transactions on Radiation and Plasma Medical Sciences, 2 (2018) 121-128.
[25] N. Kumar, J.H. Park, S.N. Jeon, B.S. Park, E.H. Choi, P. Attri, The action of microsecond-pulsed plasma-activated media on the inactivation of human lung cancer cells, Journal of Physics D: Applied Physics, 49 (2016) 115401.

[26] J.-i. Ikeda, H. Tanaka, K. Ishikawa, H. Sakakita, Y. Ikehara, M. Hori, Plasma-activated medium (PAM) kills human cancer-initiating cells, Pathology International, 68 (2018) 23-30.
[27] D. Yan, A. Talbot, N. Nourmohammadi, X. Cheng, J. Canady, J. Sherman, M. Keidar, Principles of using Cold Atmospheric Plasma Stimulated Media for Cancer Treatment, Scientific Reports, 5 (2015) 18339.
[28] H. Tanaka, M. Mizuno, F. Kikkawa, M. Hori, Interactions between a plasma-activated medium and cancer cells, Plasma Medicine, 6 (2016).
[29] J. Orth, R. Fleming, B. Palsson, Reconstruction and Use of Microbial Metabolic Networks: the Core Escherichia coli Metabolic Model as an Educational Guide, EcoSal Plus, DOI doi:10.1128/ecosalplus.10.2.1(2010).
[30] L. Heirendt, S. Arreckx, T. Pfau, S.N. Mendoza, A. Richelle, A. Heinken, H.S. Haraldsdóttir, J. Wachowiak, S.M. Keating, V. Vlasov, S. Magnusdóttir, C.Y. Ng, G. Preciat, A. Žagare, S.H.J. Chan, M.K. Aurich, C.M. Clancy, J. Modamio, J.T. Sauls, A. Noronha, A. Bordbar, B. Cousins, D.C. El Assal, L.V. Valcarcel, I. Apaolaza, S. Ghaderi, M. Ahookhosh, M. Ben Guebila, A. Kostromins, N. Sompairac, H.M. Le, D. Ma, Y. Sun, L. Wang, J.T. Yurkovich, M.A.P. Oliveira, P.T. Vuong, L.P. El Assal, I. Kuperstein, A. Zinovyev, H.S. Hinton, W.A. Bryant, F.J. Aragón Artacho, F.J. Planes, E. Stalidzans, A. Maass, S. Vempala, M. Hucka, M.A. Saunders, C.D. Maranas, N.E. Lewis, T. Sauter, B.Ø. Palsson, I. Thiele, R.M.T. Fleming, Creation and analysis of biochemical constraint-based models using the COBRA Toolbox v.3.0, Nature Protocols, 14 (2019) 639-702.
[31] I. Thiele, B.O. Palsson, A protocol for generating a high-quality genome-scale metabolic reconstruction, Nat Protoc, 5 (2010) 93-121.
[32] U. Schmitz, O. Wolkenhauer, Systems medicine, Springer2016.
[33] Z. Bodor, A.I. Fazakas, E. Kovacs, S. Lanyi, B. Albert, Systems biology and metabolic engineering for obtaining E. coli mutants capable to produce succinate from renewable resources, Romanian Biotechnological Letters, 19 (2014) 9633-9644.
[34] M.A. Campodonico, B.A. Andrews, J.A. Asenjo, B.O. Palsson, A.M. Feist, Generation of an atlas for commodity chemical production in Escherichia coli and a novel pathway prediction algorithm, GEM-Path, Metabolic Engineering, 25 (2014) 140-158.
[35] M. Das, P. Patra, A. Ghosh, Metabolic engineering for enhancing microbial biosynthesis of advanced biofuels, Renewable and Sustainable Energy Reviews, 119 (2020) 109562.
[36] K.M. Daud, M.S. Mohamad, Z. Zakaria, R. Hassan, Z.A. Shah, S. Deris, Z. Ibrahim, S. Napis, R.O. Sinnott, A non-dominated sorting Differential Search Algorithm Flux Balance Analysis (ndsDSAFBA) for in silico multiobjective optimization in identifying reactions knockout, Computers in Biology and Medicine, 113 (2019) 103390.
[37] S.R.C. Immanuel, D. Banerjee, M.P. Rajankar, A. Raghunathan, Integrated constraints based analysis of an engineered violacein pathway in Escherichia coli, Biosystems, 171 (2018) 10-19.
[38] C.P. Long, J.E. Gonzalez, N.R. Sandoval, M.R. Antoniewicz, Characterization of physiological responses to 22 gene knockouts in Escherichia coli central carbon metabolism, Metabolic engineering, 37 (2016) 102-113.
[39] E. Motamedian, M. Sarmadi, E. Derakhshan, Development of a regulatory defined medium using a system-oriented strategy to reduce the intracellular constraints, Process Biochemistry, 87 (2019) 10-16.
[40] J. Tröndle, K. Schoppel, A. Bleidt, N. Trachtmann, G.A. Sprenger, D. Weuster-Botz, Metabolic control analysis of L-tryptophan production with Escherichia coli based on data from short-term perturbation experiments, Journal of Biotechnology, 307 (2020) 15-28.
[41] X. Yang, Q. Yuan, Y. Zheng, H. Ma, T. Chen, X. Zhao, An engineered non-oxidative glycolysis pathway for acetone production in Escherichia coli, Biotechnology letters, 38 (2016) 1359-1365.
[42] X. Zhang, C.J. Tervo, J.L. Reed, Metabolic assessment of E. coli as a Biofactory for commercial products, Metabolic engineering, 35 (2016) 64-74.

[43] Y. Zheng, Q. Yuan, X. Yang, H. Ma, Engineering Escherichia coli for poly-(3-hydroxybutyrate) production guided by genome-scale metabolic network analysis, Enzyme and Microbial Technology, 106 (2017) 60-66.
[44] L.E. Sanman, Y. Qian, N.A. Eisele, T.M. Ng, W.A. van der Linden, D.M. Monack, E. Weerapana, M. Bogyo, Disruption of glycolytic flux is a signal for inflammasome signaling and pyroptotic cell death, Elife, 5 (2016) e13663-e13663.
[45] W. Shao, G. Yeretssian, K. Doiron, S. Hussain, M. Saleh, The Caspase-1 Digestome Identifies the Glycolysis Pathway as a Target during Infection and Septic Shock, The Journal of biological chemistry, 282 (2008) 36321-36329.
[46] G.R. Richards, M.V. Patel, C.R. Lloyd, C.K. Vanderpool, Depletion of Glycolytic Intermediates Plays a Key Role in Glucose-Phosphate Stress in <span class="named-content genus-species" id="named-content-1">Escherichia coli</span&gt, J Bacteriol, 195 (2013) 4816.
[47] Y. Kawai, R. Mercier, K. Mickiewicz, A. Serafini, L.P. Sório de Carvalho, J. Errington, Crucial role for central carbon metabolism in the bacterial L-form switch and killing by β-lactam antibiotics, Nat Microbiol, 4 (2019) 1716-1726.
[48] TheRegentsoftheUniversityofCalifornia, Models, http://bigg.ucsd.edu/models, (2019).
[49] D. Segrè, D. Vitkup, G.M. Church, Analysis of optimality in natural and perturbed metabolic networks, Proceedings of the National Academy of Sciences, 99 (2002) 15112.
[50] A. Varma, B.O. Palsson, Stoichiometric flux balance models quantitatively predict growth and metabolic by-product secretion in wild-type Escherichia coli W3110, Applied and environmental microbiology, 60 (1994) 3724-3731.
[51] R. Mahadevan, J.S. Edwards, F.J. Doyle, 3rd, Dynamic flux balance analysis of diauxic growth in Escherichia coli, Biophysical journal, 83 (2002) 1331-1340.
[52] J.M.H. Dirkx, H.S. van der Baan, The oxidation of glucose with platinum on carbon as catalyst, Journal of Catalysis, 67 (1981) 1-13.
[53] N.J. Kruger, A. von Schaewen, The oxidative pentose phosphate pathway: structure and organisation, Current opinion in plant biology, 6 (2003) 236-246.
[54] J.H. Freeland-Graves, C. Bavik, COENZYMES, in: B. Caballero (Ed.) Encyclopedia of Food Sciences and Nutrition (Second Edition), Academic Press, Oxford, 2003, pp. 1475-1481.
[55] D. Nayak, N. Shetti, Electrochemical Oxidation of Pro Vitamin B5, D-panthenol and its Analysis in Spiked Human Urine, Journal of Analytical Science and Technology, 7 (2016).
[56] WorthingtonBiochemicalCorporation, Glyceraldehyde-3-Phosphate Dehydrogenase, http://www.worthington-biochem.com/GAPD/, (2020).
[57] N.I. Fedotcheva, A.P. Sokolov, M.N. Kondrashova, Nonezymatic formation of succinate in mitochondria under oxidative stress, Free Radical Biology and Medicine, 41 (2006) 56-64.
[58] S.C. Thomas, A. Alhasawi, C. Auger, A. Omri, V.D. Appanna, The role of formate in combatting oxidative stress, Antonie van Leeuwenhoek, 109 (2016) 263-271.
[59] R.L. Puntel, D.H. Roos, D. Grotto, S.C. Garcia, C.W. Nogueira, J. Batista Teixeira Rocha, Antioxidant properties of Krebs cycle intermediates against malonate pro-oxidant activity in vitro: A comparative study using the colorimetric method and HPLC analysis to determine malondialdehyde in rat brain homogenates, Life Sciences, 81 (2007) 51-62.
[60] E.L. Arkblad, S. Tuck, N.B. Pestov, R.I. Dmitriev, M.B. Kostina, J. Stenvall, M. Tranberg, J. Rydström, A Caenorhabditis elegans mutant lacking functional nicotinamide nucleotide transhydrogenase displays increased sensitivity to oxidative stress, Free Radical Biology and Medicine, 38 (2005) 1518-1525.
[61] H. Hakansson, G. Vansarla, L. Marks, A. Hakansson, The human milk protein-lipid complex HAMLET disrupts glycolysis and induces death in Streptococcus pneumoniae, Journal of Biological Chemistry, 294 (2019) jbc.RA119.009930.